MOLECULAR AND CELLULAR BIOLOGY, Mar. 2009, p. 1306–1320 Vol. 29, No. 5
0270-7306/09/$08.00+0 doi:10.1128/MCB.01271-08

Raf Kinase Inhibitory Protein Function Is Regulated via a Flexible Pocket and Novel Phosphorylation-Dependent Mechanism▽†

Alexey E. Granovsky,[1]§ Matthew C. Clark,[1,2]§ Dan McElheny,[3]§ Gary Heil,[3] Jia Hong,[1,2] Xuedong Liu,[4] Youngchang Kim,[5] Grazyna Joachimiak,[5] Andrzej Joachimiak,[5] Shohei Koide,[3]§ and Marsha Rich Rosner[1,2]§*

Ben May Department for Cancer Research,[1] Department of Neurobiology, Pharmacology, and Physiology,[2] and Department of Biochemistry and Molecular Biology,[3] University of Chicago, Chicago, Illinois 60637; Department of Chemistry and Biochemistry, University of Colorado—Boulder, Boulder, Colorado 80309[4]; and Structural Biology Center, Biosciences Division, Argonne National Laboratory, Argonne, Illinois[5]

Received 11 August 2008/Returned for modification 10 October 2008/Accepted 15 December 2008

Raf kinase inhibitory protein (RKIP/PEBP1), a member of the phosphatidylethanolamine binding protein family that possesses a conserved ligand-binding pocket, negatively regulates the mammalian mitogen-activated protein kinase (MAPK) signaling cascade. Mutation of a conserved site (P74L) within the pocket leads to a loss or switch in the function of yeast or plant RKIP homologues. However, the mechanism by which the pocket influences RKIP function is unknown. Here we show that the pocket integrates two regulatory signals, phosphorylation and ligand binding, to control RKIP inhibition of Raf-1. RKIP association with Raf-1 is prevented by RKIP phosphorylation at S153. The P74L mutation increases kinase interaction and RKIP phosphorylation, enhancing Raf-1/MAPK signaling. Conversely, ligand binding to the RKIP pocket inhibits kinase interaction and RKIP phosphorylation by a noncompetitive mechanism. Additionally, ligand binding blocks RKIP association with Raf-1. Nuclear magnetic resonance studies reveal that the pocket is highly dynamic, rationalizing its capacity to interact with distinct partners and be involved in allosteric regulation. Our results show that RKIP uses a flexible pocket to integrate ligand binding- and phosphorylation-dependent interactions and to modulate the MAPK signaling pathway. This mechanism is an example of an emerging theme involving the regulation of signaling proteins and their interaction with effectors at the level of protein dynamics.

Raf kinase inhibitory protein (RKIP/PEBP1) is a signaling modulator that regulates key signal transduction cascades in mammalian cells (reviewed in reference 16). A negative regulator of mitogen-activated protein kinase (MAPK) signaling (42), RKIP inhibits Raf kinase by binding directly to Raf-1, thereby preventing the phosphorylation and activation of Raf-1 (8, 38). RKIP functions as a regulator of the spindle checkpoint and promotes genomic stability by preventing MAPK from inhibiting Aurora B kinase (10). Consistent with this role, RKIP suppresses lung metastasis by prostate tumor cells in an orthotopic murine model (15). RKIP may be a general metastasis suppressor for solid tumors, since RKIP expression is low or undetectable in prostate and breast tumors, melanoma, hepatocellular carcinoma, and colorectal tumors (1, 2, 14, 15, 19, 34). Finally, RKIP suppresses NF-κB activation (43), inhibits G protein-coupled receptor (GPCR) kinase 2 (GRK2)-mediated downregulation of GPCRs (28), and potentiates the efficacy of chemotherapeutic agents (5). Thus, RKIP regulates three key mammalian signaling pathways involving MAPK, GPCR, and NF-κB signaling.

RKIP is a member of the phosphatidylethanolamine binding protein (PEBP) family, which extends from bacteria to humans and consists of more than 400 proteins (16, 33). X-ray crystallographic studies have demonstrated that highly conserved sequences cluster around a pocket capable of binding anions, including *o*-phosphorylethanolamine (PE), acetate, and cacodylate (3, 35). This pocket is the only clearly identifiable feature for potential ligand binding within the RKIP architecture. Although the ligand-binding pocket shares homology with phospholipid binding domains, PEBP associates with phospholipid membranes primarily via peripheral, ionic interactions rather than more integrally inserting itself into the membrane (reference 39 and data not shown). The fact that RKIP interacts with protein targets such as Raf-1 and is phosphorylated by other protein kinases raises the possibility that the pocket mediates protein-protein interactions.

The physiological role of the ligand-binding pocket is illustrated by studies of plant and yeast PEBPs. In the plant homologue of RKIP, mutation of the conserved DPDxP motif within the pocket (the equivalent of P74L) causes tomato plants to switch developmentally from shoot growth to flowering (32). The *Saccharomyces cerevisiae* RKIP/PEBP homologue, Tfs1p, functions as a negative regulator of RasGAP (Ira2), leading to upregulation of yeast Ras, activation of adenylyl cyclase, and increased cyclic AMP activation of protein kinase A (6). Yeast Ras signaling is inhibited by the corresponding P74L mutation in the pocket of Tfs1p, blocking Tfs1p interaction with Ira2. These results highlight the functional

* Corresponding author. Mailing address: Gordon Center for Integrative Sciences, 929 East 57th Street, Chicago, IL 60637. Phone: (773) 702-0380. Fax: (773) 702-4476. E-mail: m-rosner@uchicago.edu.

§ M.C.C., A.E.G., and D.M. contributed equally to this work. S.K. and M.R.R. contributed equally as senior authors.

† Supplemental material for this article may be found at http://mcb.asm.org/.

▽ Published ahead of print on 22 December 2008.

importance of the pocket among eukaryotic RKIP/PEBP family members. However, the molecular mechanism by which the pocket influences RKIP function and the significance of ligand binding to the pocket are unknown.

Previous work has established the phosphorylation-mediated control of RKIP function. RKIP binds Raf-1, inhibiting Raf-1 activation and consequent signaling to MAPK (38, 42). When RKIP residue S153 is phosphorylated by protein kinase C (PKC), which occurs following cell stimulation with growth factors such as epidermal growth factor (EGF) or serum, RKIP can no longer bind to Raf-1, and thus it is inactivated as a Raf-1 inhibitor (8). Phosphorylation at S153 promotes the association of RKIP with, and inhibition of, GRK2, a kinase that phosphorylates and downregulates GPCRs such as the β-adrenergic receptor (28). Thus, S153 phosphorylation of RKIP is a key regulatory element of its association with and inhibition of different targets. The importance of the pocket and that of S153 phosphorylation have been independently established, but it is not clear whether these regulatory elements are functionally linked. Addressing this question is important for advancing our understanding of the molecular mechanism of RKIP function, which is likely to be pertinent to many RKIP/PEBP family members.

In the present study, using cellular, biochemical, and structural approaches, we demonstrate that the highly conserved ligand-binding pocket integrates two regulatory signals, phosphorylation and ligand binding, to control RKIP function. Our results suggest that, in contrast to the mechanisms for other pocket-containing single-domain proteins, the structure and/or dynamics of the pocket influences RKIP interaction with and phosphorylation by kinases. This mechanism is likely conserved among RKIP homologues in eukaryotes.

MATERIALS AND METHODS

Mammalian plasmid production. Full-length wild-type (wt) rat RKIP (residues 1 to 187; 23 kDa) was expressed with a hemagglutinin (HA) tag in a pCR3.1 vector (pCR-HA-RKIP) as previously described (8). The HA-tagged RKIP(P74L) plasmid was made using the QuikChange (Stratagene) site-directed mutagenesis kit, with confirmation of the mutation by cDNA sequence analysis in both directions. The HA-RKIP(P74L S153V) mutant was obtained by inserting a KpnI-PmlI fragment of the HA-RKIP(P74L) mutant into the similarly digested HA-RKIP(S153V) construct (8). The pRav-Flag-Raf-1 plasmid (TAP-Raf-1) was constructed by cloning a PCR product containing the full-length Raf-1 sequence generated from pCMV-Raf-1 into the XhoI site of the pRav-Flag plasmid (23).

Cell culture. The stable short hairpin RNA (shRNA) 293 and 293T cell lines in which endogenous RKIP was depleted (termed HshRKIP 293 and HshRKIP 293T, respectively) (38) were grown at 37°C in Dulbecco's modified Eagle medium (DMEM) with 10% fetal bovine serum, 50 U/ml penicillin, and 50 μg/ml streptomycin, and selection was maintained with 2 μg/ml puromycin. Cells were serum starved overnight at 37°C in DMEM prior to treatment. The immortalized H19-7 cell line from embryonic rat hippocampal cells (11) was maintained in 10% fetal bovine serum, 50 U/ml penicillin–50 μg/ml streptomycin, and 200 μg/ml G418 at 33°C. Cells were serum starved at 39°C in N2 medium or DMEM overnight prior to treatment. To make a stable TAP-Raf-1 (Raf-1 with a tandem affinity purification tag using protein A and a Flag tag) H19-7 cell line, the Phoenix-Ampho packaging cell line was transfected with the vector for virus production. H19-7 cells were exposed three to five times to virus-containing supernatants, and cells stably expressing TAP-tagged Raf-1 were obtained by cell sorting according to their green fluorescent protein levels.

MAPK activation and RKIP phosphorylation assays. 293 or 293T cells stably depleted of endogenous RKIP (HshRKIP 293 and HshRKIP 293T cells) were seeded in 12-well plates at 4×10^4 per well for MAPK activation assays and the RKIP phosphorylation assay. For in vitro PKC or MAPK assays, enzymes were incubated in 50 μl of reaction buffer. HshRKIP 293 or HshRKIP 293T cells were transfected with 2 μg DNA the following day, with pcDNA transfection for the control (no RKIP). To assess RKIP depletion, RKIP phosphorylation, and MAPK activation, at 24 h posttransfection cells were serum starved overnight and either treated with 10 ng/ml EGF (Bio-Medical Technologies, Inc.) for 5 min, 400 nM tetradecanoyl phorbol acetate (TPA; Sigma) for 15 min, or 800 nM TPA for 15 min (RKIP phosphorylation assay) or left untreated. Cells were lysed in Triton X-100 lysis buffer (1% Triton X-100, 1 mM EDTA, 150 mM NaCl, 50 mM NaF, and a protease inhibitor mixture [Calbiochem]). Thirty micrograms of cell lysate was resolved by sodium dodecyl sulfate-polyacrylamide gel electrophoresis (SDS-PAGE), transferred to nitrocellulose membranes, and analyzed by immunoblotting with an anti-α-tubulin (Santa Cruz Biotechnology, Inc.), anti-phospho-extracellular signal-regulated kinase (anti-phospho-ERK) (Cell Signaling Technology, Inc.), or anti-RKIP (8) antibody. Immunoreactivity was digitally analyzed using an imaging system and software from Alpha Innotech Corp.

Protein production. Rat wt RKIP was overexpressed in *Escherichia coli* BL21/pLysS (Novagen) harboring the pGEX2T vector containing the RKIP cDNA. Mutations (S153E, H86A, P74L, S153V, and P74L S153V) were introduced by QuikChange mutagenesis (Stratagene) or subcloned from the corresponding HA-RKIP constructs and were confirmed by DNA sequencing. RKIP was purified using glutathione-Sepharose 4B chromatography (Amersham). The glutathione *S*-transferase (GST) tag was cleaved with biotinylated thrombin (Novagen) and removed with glutathione-Sepharose 4B, and the biotinylated thrombin was removed using streptavidin agarose beads (Novagen). The calmodulin-binding peptide (CBP)-tagged Raf-1 kinase domain was expressed in *Escherichia coli* BL21(DE3)/pLysS (Novagen) containing the pCAL-n-Raf-CR3 plasmid (a gift from M. Marshall, Eli Lilly & Company). CBP-Raf1 was purified using calmodulin affinity resin (Stratagene) as previously described (22). A plasmid for bacterial expression of activated His_6-tagged phospho-ERK2 (pERK2) was kindly provided by M. Cobb (University of Texas Southwestern Medical Center). His_6-pERK2 was expressed and purified as previously described (41).

In vitro kinase assays. In vitro phosphorylation of RKIP by PKCα was tested using 100 ng of baculovirus-derived PKCα (Panvera) in 50 μl of kinase buffer (20 mM HEPES [pH 7.4], 100 μM $CaCl_2$, 10 mM $MgCl_2$, 100 μg/ml L-α-phosphatidylserine, and 20 μg/ml diacylglycerol). For testing the effects of 1,2-dihexanoyl-*sn-glycero*-3-phosphoethanolamine (DHPE), L-α-phosphatidylserine was omitted in the kinase buffer. For these assays, GST-cleaved, monomeric RKIP samples were used. Phosphorylation of RKIP by MAPK used 25 U of activated p42 kinase (New England Biolabs) in 50 μl of 1× kinase reaction buffer supplied with enzyme. The time course assay mixture contained 2.5 μg of the indicated RKIP, and the mixture for the kinase assay in the presence of various concentrations of DHPE contained 5 μg RKIP. The reactions were started by the addition of 100 μM ATP containing 5 μCi of [γ-^{32}P]ATP, carried out at 30°C for 10 min (or for the indicated time in the time course assays), and then stopped by the addition of 6× SDS-PAGE sample buffer and heating at 100°C for 5 min. The samples were separated on a 12% acrylamide gel, transferred to a nitrocellulose membrane, and visualized by exposure to film. Results were subsequently quantified using phosphorimager screens on a Molecular Dynamics PhosphorImager with ImageQuant software, and membranes were immunoblotted after [γ-^{32}P]ATP decay with an anti-RKIP antibody (8). Specific activity was determined by comparing the extent of phosphate transfer to RKIP/min · mg protein under V_{max} conditions to that of standard proteins (histone H1 for PKC and MBP for ERK2) with known phosphate transfer rates.

Raf-RKIP binding assay. To assay association, stably expressed TAP-Raf-1 was immunoprecipitated from H19-7 cells starved overnight in serum-free DMEM, and TAP-Raf-1 was isolated on immunoglobulin G (IgG)-Sepharose beads. Cells were lysed in TAP lysis buffer (10 mM HEPES [pH 7.4], 3 mM $MgCl_2$, 10 mM KCl, 5% glycerol, 0.1% NP-40) and cleared by centrifugation. The cell lysate was combined with IgG-Sepharose beads that were preequilibrated TAP lysis buffer (Amersham Biosciences) and was incubated for 1 h at 4°C. Beads were washed with TAP lysis buffer and then equilibrated with binding buffer (10 mM HEPES [pH 7.4], 3 mM $MgCl_2$, 10 mM KCl, 150 mM NaCl). Beads were aliquoted, combined with 5 μg of RKIP and various concentrations of DHPE, and then incubated for 30 min at 4°C. The complex was washed three times with cold binding buffer containing corresponding concentrations of DHPE and was then boiled in 2× sample buffer for 1 min. The proteins were separated on 12% polyacrylamide gels and stained with Coomassie blue or were transferred to nitrocellulose membranes and immunoblotted with anti-RKIP antibodies.

For the in vitro GST-binding assay, glutathione-Sepharose 4B was blocked with 10% normal goat serum followed by incubation with 5 μg of GST or GST-RKIP. Coupled GST fusion proteins were then incubated with 10 μg of CBP-Raf1 and various concentrations of DHPE for 30 min at 4°C, followed by

extensive washing in a buffer (20 mM Tris [pH 7.4], 150 mM NaCl, and corresponding concentrations of DHPE), and were boiled in 2× sample buffer for 1 min. Bound proteins were resolved on a 10% acrylamide gel, transferred to nitrocellulose membranes, and immunoblotted with anti-c-Raf antibodies (Santa Cruz).

Protein preparation for crystallography and nuclear magnetic resonance (NMR) spectroscopy. BL21(DE3) cells (Novagen) harboring a pMCSG7-derived expression vector (37) for rat RKIP were grown at 37°C in M9 medium with either no supplement, $^{15}NH_4Cl$ as the sole nitrogen source, or, for ^{13}C- and ^{15}N-enriched samples, [U-^{13}C]glucose as the sole carbon source. The expression construct consisted of a His_6 tag fused in frame with a tobacco etch virus protease cleavage signal and the entire open reading frame (encoding residues 1 to 187) of rat RKIP. Protein expression was induced with 0.2 mM isopropyl-1-thio-β-D-galactoside (IPTG) when the optical density at 600 nm of cultures reached ~0.7, and expression was allowed to proceed for 16 h at 30°C.

His-tagged RKIP was purified using a Ni affinity column (Ni Sepharose 6 Fast Flow; Amersham) as described previously (20). His-RKIP was cleaved with His-tagged tobacco etch virus protease as previously described (29), and cleaved RKIP was purified by passing the cleavage product through a nickel affinity column. The sample purity was >95% as judged by SDS-PAGE. RKIP mutants were expressed and purified in the same manner. NMR samples were made in 50 mM Tris-HCl (pH 7.4) containing 100 mM NaCl and 7% D_2O.

Protein crystallization. RKIP(S153E) was crystallized in vapor diffusion hanging drops by mixing 1 ml of protein in 10 mM Tris (pH 7.4)–50 mM NaCl–1 mM dithiothreitol–10 mM PE–2 mM GTP, at a 27.4-mg/ml concentration, with 1 ml of 0.1 M sodium acetate trihydrate (pH 4.5) and 25% (wt/vol) polyethylene glycol (PEG) 3350. Samples were equilibrated at 4°C over 500 μl of the precipitant solution. Crystals appeared in approximately 2 weeks. Crystals were flash frozen in liquid nitrogen with crystallization buffer plus 28% sucrose as a cryoprotectant prior to data collection.

wt RKIP was crystallized in vapor diffusion sitting drops by mixing 400 nl of protein in 50 mM NaCl–10 mM Tris (pH 8.0)–1 mM dithiothreitol–5 mM DHPE, at a 27-mg/ml concentration, with 400 nl of 0.2 M $CaCl_2$, 0.1 M HEPES (pH 7.5), and 30% (wt/vol) PEG 4000 in a 96-well format plate. Samples were equilibrated at 4°C over a 145-ml reservoir of the precipitant solution. Crystals appeared after 4 to 5 days and were flash frozen in liquid nitrogen with crystallization buffer with 35% (wt/vol) PEG 4000 as a cryoprotectant prior to data collection.

Diffraction data collection and structure determination and refinement. All diffraction data were collected at 100 K at the Structural Biology Center, at the Advanced Photon Source, Argonne National Laboratory. Details of data collection and statistics are available on request. Both structures were determined by molecular replacement. Details of structure determination procedures and crystallographic statistics are available on request.

NMR measurements. RKIP resonance assignments have been determined recently and can be accessed through BMRB entry 6783 (7). All NMR spectra were acquired at 30°C on an Inova 600-MHz spectrometer equipped with a cryogenic triple-resonance probe. Residual dipolar coupling values were determined on RKIP samples placed in neutral 4% (wt/vol) stretched acrylamide gels using pulse sequences in the Varian BioPack suite. Additional details are available on request.

Ligand-binding assays. Ligand stocks were prepared in the NMR buffer described above, and the pH value was adjusted appropriately. NMR samples for ligand binding contained 75 mM ^{15}N-labeled RKIP. $^{1}H,^{15}N$ heteronuclear single-quantum correlation (HSQC) spectra (21) of ^{15}N-labeled RKIP in the presence of the various ligands were acquired at 30°C. Exact peak positions and intensities were obtained using 2-dimensional deconvolution of peak positions with the pkfit program. Global fitting analysis of peak positions and intensities was performed using the GLOVE program (J. C. Lansing, K. Sugase, H. J. Dyson and P. E. Wright, unpublished data) modified to fit the data to a single-site binding model.

NMR structure calculations. Distance restraints were determined using the AUTOSTRUCTURE suite (44). The f dihedral restraints were derived primarily on $^{3}J\ H^{N}H^{a}$ coupling constants and also from ^{13}C chemical shifts using TALOS (9). Structural refinement was performed in AMBER8 (http://ambermd.org/). Additional details, statistics of experimental restraints, and calculated structures are available on request.

^{15}N relaxation measurements and data analysis. ^{15}N T_1, T_2, and {^{1}H}-^{15}N nuclear Overhauser effects were measured at 30.4°C (calibrated with undiluted methanol) on Varian Inova spectrometers operating at proton Larmor frequencies of 600.9 MHz and 499.7 MHz. The relaxation data were acquired using previously described methods (13, 18). Model-free calculations (27) were performed using the Model-free program, version 4.15, provided by A. G. Palmer III (Columbia University, New York, NY). Additional details are available on request.

SPR. The binding affinity and the kinetics of interactions between His_6-pERK2 and either GST-wt RKIP or GST-RKIP(P74L) were measured with a BIAcore 3000 biosensor through surface plasmon resonance (SPR). His_6-ERK2 was immobilized on a nickel-nitrilotriacetic acid-containing sensor chip at a flow rate of 5 μl/min. To prepare the control surface, running buffer was injected instead of $NiCl_2$ solution before the injection of His_6-ERK2. GST-wt RKIP or GST-RKIP(P74L) at various concentrations was injected over both the immobilized His_6-pERK surface and the control surface. To determine the effect of DHPE on RKIP-ERK2 interaction, GST-wt RKIP or GST-RKIP(P74L) was injected in the presence of various DHPE concentrations. The concentrations of wt and mutant RKIP in these experiments were lower than the K_d (dissociation constant) values for RKIP-ERK2 or RKIP(P74L)-ERK2 interactions, respectively. The amount of RKIP bound to the sensor chip was measured by the change in the refractive index (shown in arbitrary response units). All kinetic experiments were performed at 4°C in HBS (10 mM HEPES [pH 7.4], 0.15 M NaCl, 50 μM EDTA, 0.05% Tween 20) using flow rates of 20 μl/min. After each binding experiment, the sensor chip was regenerated by washing with 80 μl of 0.3 M imidazole–0.5 M NaCl, followed by 80 μl of 0.35 M sodium EDTA in HBS. Duplicate injections of each concentration of RKIP or its mutant were performed.

The data were analyzed using BIAevaluation (version 4.1) software. Sensorgram association and dissociation curves were locally or globally fit to one-site binding models. Binding curves were generated by plotting arbitrary response units at the end of the binding phase of each sensorgram (115 s from the start of injection).

Protein structure accession numbers. Atomic coordinates of the rat RKIP containing the S153E mutation complexed with PE and of the wt rat RKIP apoprotein (apo-RKIP) have been deposited in the Protein Data Bank (PDB) as 2IQX and 2IQY, respectively.

RESULTS

The P74L mutation inactivates RKIP as a Raf-1 inhibitor by making it a better kinase substrate. We first examined the mechanism by which the P74L mutation affects RKIP function. We selected this mutation because of the dramatic developmental switch caused by an equivalent mutation in the plant homologue as described above. RKIP phosphorylation at S153 by PKC prevents interaction between RKIP and Raf-1 (8) and consequently promotes ERK1 and ERK2 (ERK1,2) signaling. The P74L mutation of the RKIP pocket also enhanced EGF-stimulated activation of MAPK (ERK1,2) (Fig. 1A) and DNA synthesis (38) (Fig. 1B). We observed a significant increase in S153 phosphorylation in cells transfected with RKIP(P74L) relative to those transfected with wt RKIP when the cells were stimulated with TPA, a PKC activator, or with EGF (Fig. 1C; see also Fig. S1A in the supplemental material). Comparable results were obtained with another pocket mutant (H86A) (data not shown), containing a mutation that also inhibits the yeast homologue, Tfs1p (6). Upon EGF receptor stimulation, RKIP is phosphorylated by PKC at the plasma membrane (Fig. 1D). Increased phosphorylation at S153 of the P74L mutant was found relative to that of wt RKIP after EGF treatment (Fig. 1D). These results clearly indicate that mutations in the pocket influence the function of RKIP as a Raf-1 inhibitor as well as the properties of RKIP as a kinase substrate.

To determine whether S153 phosphorylation was responsible for the loss of RKIP function triggered by the P74L mutation, we expressed the double mutant RKIP(P74L S153V). The additional S153V mutation eliminated RKIP phosphorylation at this site (Fig. 1C) and rescued RKIP inhibition of ERK activation (Fig. 1E), indicating that RKIP(P74L) in the absence of S153 phosphorylation is an active Raf-1 inhibitor and that the inactivation of this RKIP function by the P74L

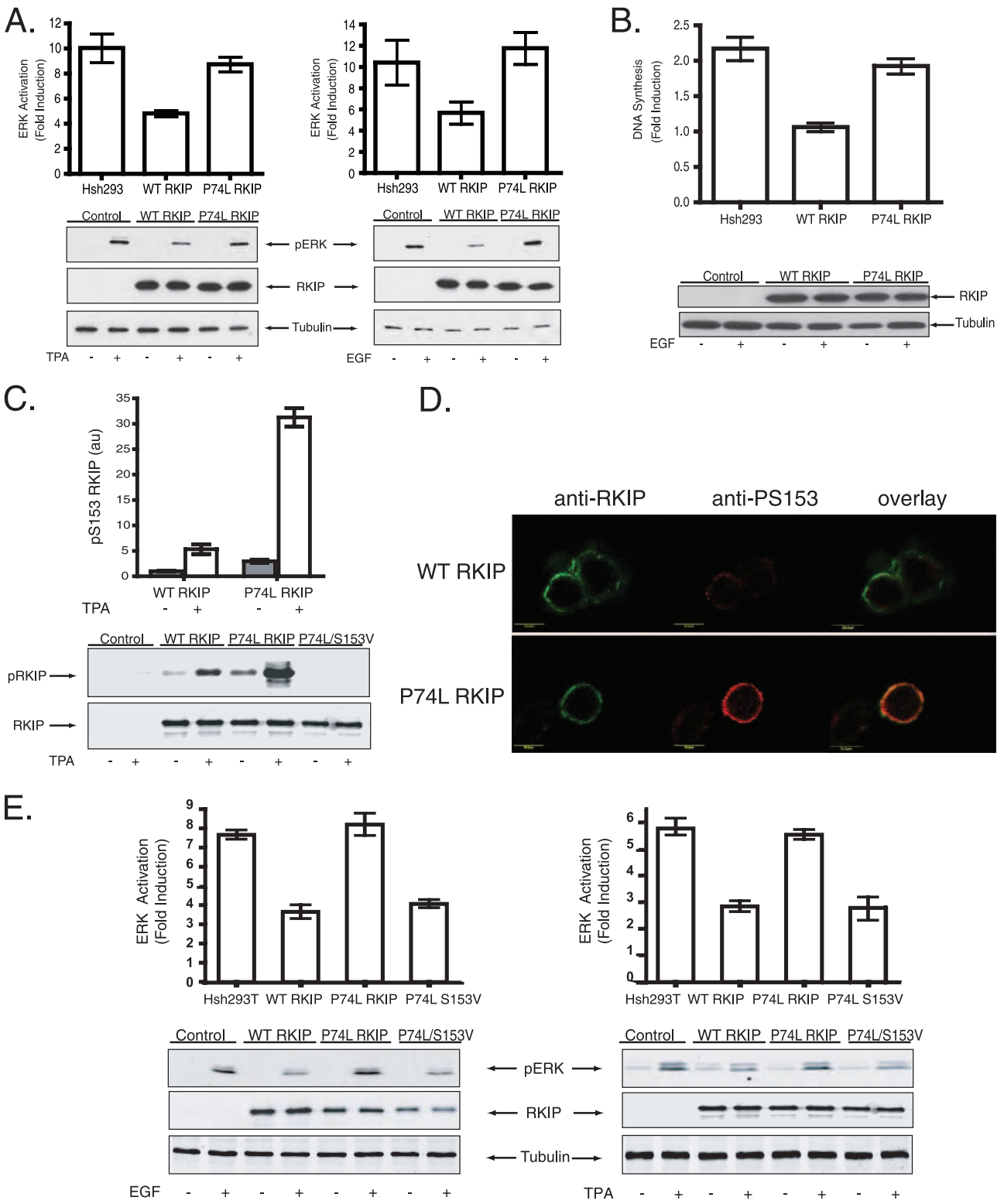

FIG. 1. The RKIP(P74L) mutation blocks RKIP inhibition of MAPK and DNA synthesis and increases S153 phosphorylation in cells. (A) 293 cells stably depleted of human RKIP with shRNA (HshRKIP cells) were transfected with wt RKIP or RKIP(P74L). Cells were stimulated with 400 nM TPA (left) or 10 ng/ml EGF (right), and lysates were immunoblotted with an anti-pERK, anti-RKIP, or antitubulin antibody. (Top) Graphs of results from three independent experiments ± standard deviations. (Bottom) Representative Western blots. (B) Cells were stimulated with 10 ng/ml EGF and assayed for DNA synthesis as measured by bromodeoxyuridine incorporation. (Top) Graph of results from four independent experiments ± standard deviations. (Bottom) Representative Western blot. (C) Phosphorylation of RKIP at S153 in HshRKIP 293T cells transfected with wt RKIP, RKIP(P74L), or RKIP(P74L S153V) and stimulated with 400 nM TPA. (Top) Graph of results from three independent experiments ± standard deviations. (Bottom) Lysates were immunoblotted with anti-pS153 and anti-RKIP antibodies. (D) HshRKIP 293 cells transiently transfected with wt RKIP or RKIP(P74L) were fixed and immunostained with an anti-RKIP (green) or anti-pS153 (red) antibody. (E) HshRKIP 293T cells were transfected with wt RKIP, RKIP(P74L), or RKIP(P74L S153V). Cells were stimulated with 400 nM TPA (right) or 10 ng/ml EGF (left), and lysates were immunoblotted with an anti-pERK, anti-RKIP, or anti-tubulin antibody. (Top) Graphs of results from three independent experiments ± standard deviations. (Bottom) Representative Western blots.

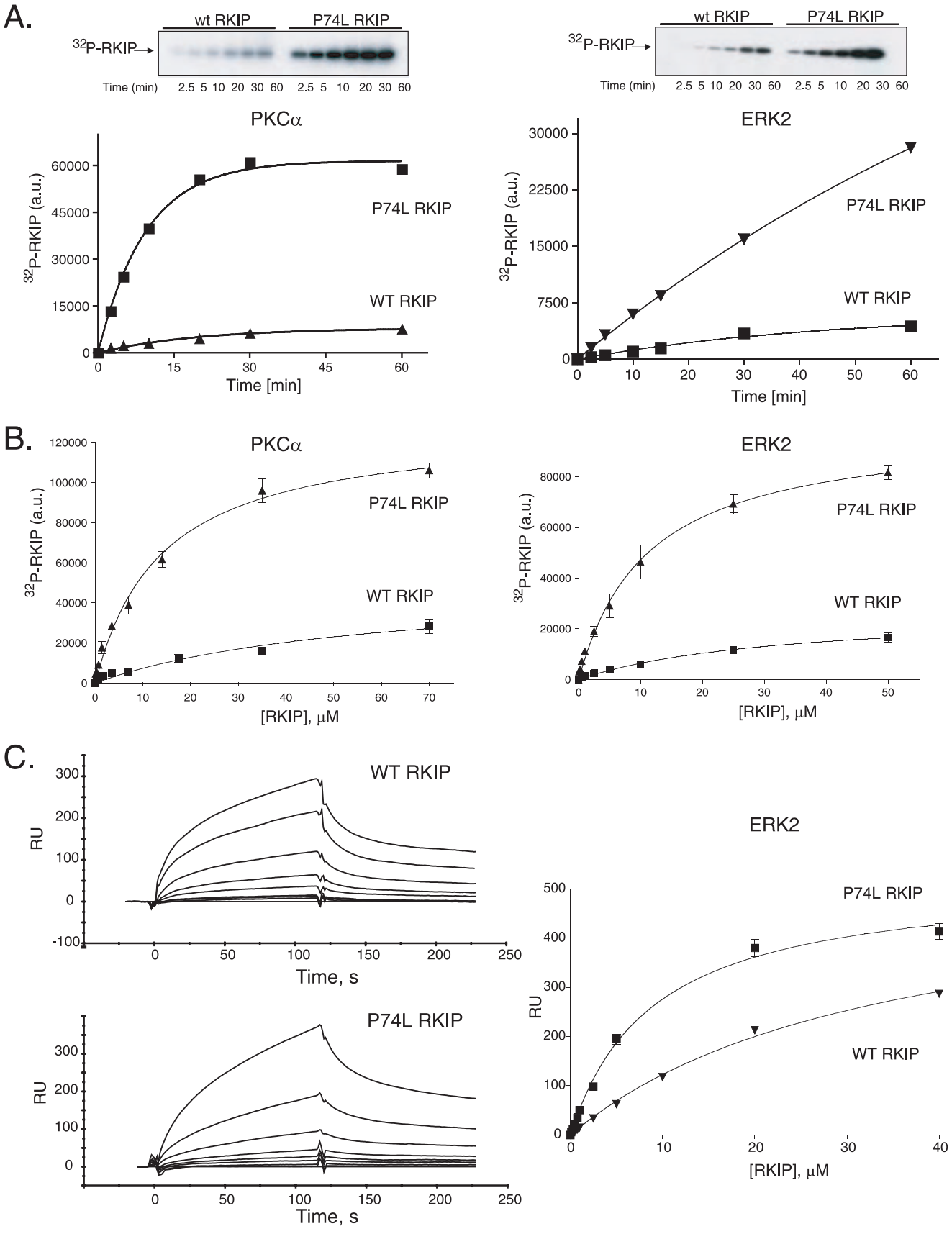
A.
wt RKIP
P74L RKIP
32P-RKIP
Time (min) 2.5 5 10 20 30 60 2.5 5 10 20 30 60
PKCα
32P-RKIP (a.u.)
P74L RKIP
WT RKIP
Time [min]
ERK2
B.
[RKIP], μM
C.
WT RKIP
P74L RKIP
RU
Time, s

mutation was not due to nonspecific or denaturing structural changes. Thus, the RKIP P74L mutation inactivates RKIP as a Raf-1 inhibitor in cells through enhancement of S153 phosphorylation. A similar, phosphorylation-dependent mechanism could explain previous observations that pocket mutations of yeast Tsfp1 abolish binding to its target (6).

In vitro characterization revealed that the increased S153 phosphorylation by PKC reflected an intrinsic property of mutant RKIP independent of the cellular context. As in cells, phosphorylation of the P74L mutant by PKC in vitro was greater in terms of both the initial rate and the final amount of product than that of wt RKIP at the same starting substrate concentration (Fig. 2A). The P74L mutation caused a ~4.2-fold decrease in the K_m [57.3 ± 15.5 μM for wt RKIP and 13.8 ± 1.6 μM for RKIP(P74L)] and a ~4.5-fold increase in the V_{max} [15.1 ± 2.6 nmol/min · mg for wt RKIP and 69.2 ± 4.7 nmol/min · mg for RKIP(P74L); units refer to nanomoles of phosphate transferred to the substrate per minute per milligram of enzyme] relative to those of wt RKIP (Fig. 2B). Increases in both the enzyme-substrate affinity and the catalytic rate could explain the increase in the amount of phosphorylated product, and the more-rapid turnover is probably due to faster release of the phosphorylated product from PKC. Other kinases also phosphorylate RKIP(P74L) to a greater extent than wt RKIP (Fig. 2 and data not shown). For example, ERK2 phosphorylation of RKIP at T42 is enhanced by the P74L mutation (Fig. 2A and B). As with PKC phosphorylation of S153, the P74L mutation decreased the K_m for ERK2 phosphorylation ~3-fold [32.0 ± 7.8 μM for wt RKIP versus 11.1 ± 1.4 μM for RKIP(P74L)] and increased the V_{max} of T42 phosphorylation by ERK2 ~4-fold [950 ± 116 pmol/min · mg for wt RKIP versus 3,600 ± 160 pmol/min · mg for RKIP(P74L)] relative to those for wt RKIP. Thus, the P74L pocket mutation increases the rate of RKIP phosphorylation by PKC and ERK2.

To investigate the RKIP-kinase interactions in more detail, we analyzed the binding of both wt RKIP and RKIP(P74L) to kinases by using SPR. We chose to focus on the RKIP interaction with ERK2, since PKC requires a phospholipid cofactor that could complicate interpretation of the results (see below). A higher affinity (i.e., lower K_d values) was observed for the P74L mutant than for wt RKIP, reflecting changes in both association and dissociation rates (Fig. 2C; also data not shown) [K_d, 44.6 ± 11.1 μM for wt RKIP and 7.1 ± 0.8 μM for RKIP(P74L)]. Similar changes in K_d values were observed by analyzing these interactions under steady-state conditions (Fig. 2C, right) [K_d, 54.6 ± 11.8 μM for wt RKIP versus 4.4 ± 0.2 μM for RKIP(P74L)]. These K_d values are consistent with the K_m values revealed in the phosphorylation assays. Together, the phosphorylation and binding data demonstrate that the P74L mutant enhances the affinity of RKIP for two kinases that phosphorylate RKIP at different sites, suggesting that the pocket constitutes part of an interaction interface that is utilized by multiple kinases that phosphorylate RKIP.

X-ray crystallography and NMR spectroscopy show no direct structural cross talk between the S153 and P74 sites. To determine whether the P74L pocket mutation alters the phosphorylation of S153 by directly perturbing the conformation of S153 and its vicinity, we investigated whether there is a structural linkage between the S153 residue and the P74 site. Although we have not been able to crystallize the P74L mutant, rat RKIP with a phosphomimetic S153-to-glutamic acid mutation (Fig. 3A) in complex with PE, a lipid head group, was crystallized at an acidic pH, and the structure was compared to that of the wt apo-RKIP crystallized at a neutral pH. Data collection and crystallographic statistics are available on request. The two structures are nearly identical except for small differences at the C terminus (Fig. 3B), and they are very similar to the previously determined structures of RKIP/PEBP1 from other vertebrates, including the conservation of two *cis* peptide bonds (between residues 73 and 74 and between residues 82 and 83) (3, 35). The crystallographic data indicate that the S153E mutation causes no major structural perturbations, and the S153E and P74 regions of the protein are approximately 20 Å apart.

Although no direct structural interactions between the pocket residue (P74) and S153E were revealed by crystallography, more-subtle perturbations could theoretically link the two sites in solution. To test this possibility, we analyzed the effects of mutations at these sites by NMR. The $^{1}H,^{15}N$ HSQC spectrum provides site-specific probes for amide moieties in a ^{15}N-enriched protein. Since all amino acid residues except for prolines include an amide moiety, HSQC signals detect conformational changes at an amino acid residue resolution (7, 36). We have completed sequence-specific resonance assignments of wt RKIP (7), and thus a perturbed HSQC signal can be unambiguously assigned to an RKIP residue. A comparison of the HSQC spectra of wt RKIP, the negatively charged S153E mutant that more closely resembles phosphorylated S153, and the P74L mutant (Fig. 3D and E; see also Fig. S2 in the supplemental material) revealed that a majority of peaks were unaffected by these mutations, indicating that the mutants retained the overall structure. As in previous structures, the amide bond between A73 and P74 in our crystal structures

FIG. 2. Effect of a pocket mutation on the interaction of RKIP with PKC and MAPK in vitro. (A) Time course of PKC (left) and MAPK (right) phosphorylation of wt RKIP and RKIP(P74L). Kinase reactions were conducted as described in Materials and Methods, and aliquots from each reaction mixture were taken at the indicated times. (Top) Representative Western blot; (bottom) graph of results from three independent experiments ± standard deviations. a.u., arbitrary units. (B) PKC (left) and MAPK (right) kinase assays using increasing concentrations of bacterially expressed wt RKIP and RKIP(P74L) as substrates. Shown are graphs of results from three independent experiments ± standard deviations. (C) Analysis of ERK2 binding to RKIP. (Left) Kinetic interactions between activated His_6-ERK2 and GST-wt RKIP or GST-RKIP(P74L), monitored by SPR in a Biacore 3000 apparatus. GST-wt RKIP or GST-RKIP(P74L) was injected at concentrations ranging from 100 to 15,000 nM. The association and dissociation phases were monitored for 120 s. The association rate (k_a) and K_d values for wt RKIP, calculated using global fitting analysis, were 260 ± 6 M^{-1} s^{-1} and 1.1e^{-2} ± 6.7e^{-5} s^{-1}, respectively. The k_a and K_d values for RKIP(P74L), calculated using global fitting analysis, were 593 ± 15 M^{-1} s^{-1} and 4.2e^{-3} ± 1.2e^{-5} s^{-1}, respectively. (Right) The arbitrary response units (RU) at the 115-s point during association phases were plotted using a one site-binding equation. The graph shows results from two independent experiments ± ranges.

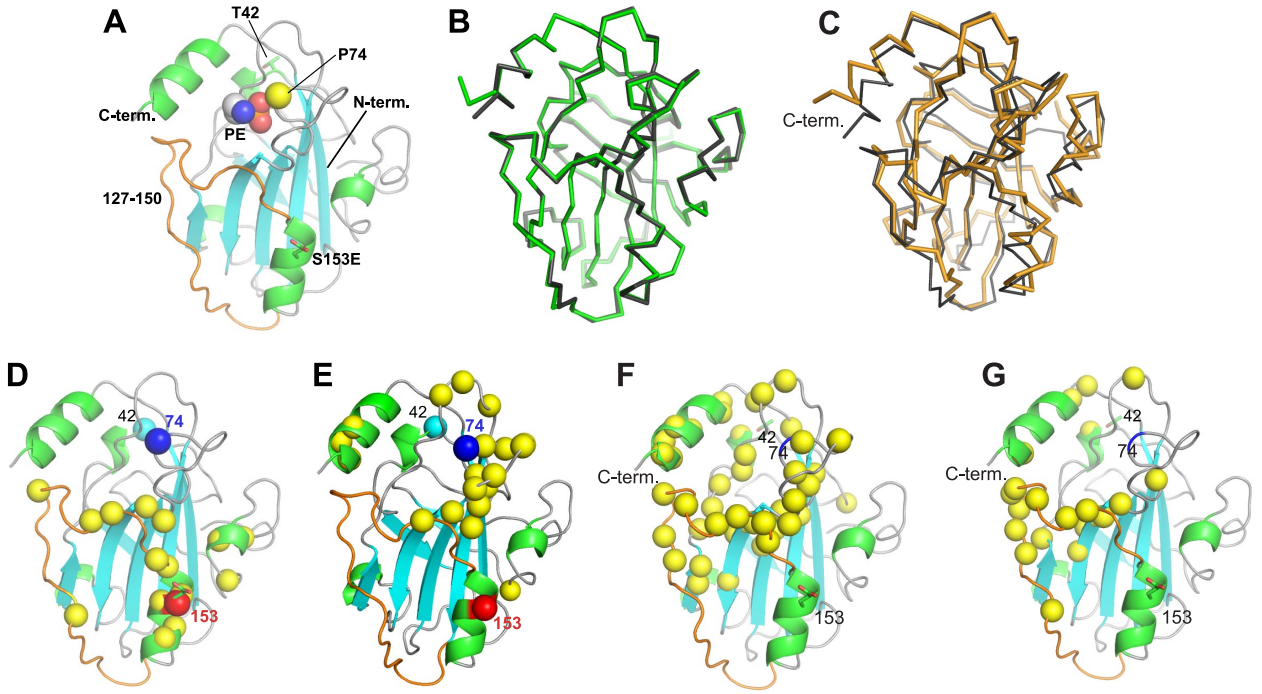

FIG. 3. X-ray crystal structures of rat RKIP, its solution NMR structure, and structural perturbations caused by mutations and ligand binding as probed by NMR spectroscopy. (A) Cartoon representation of the X-ray crystal structure of RKIP(S153E) in complex with PE. PE is shown as spheres. The mutated site, S153E, is shown as stick models; the Ca atom of P74 is represented by a yellow sphere; and residues 140 to 150 are shown in orange. The N and C termini (term.) are also indicated. (B) Superposition of wt apo-RKIP (green) and RKIP(S153E) (gray) in complex with PE. Both structures are shown as Ca traces. The Ca root mean square distance is 0.29 Å. Residue 187 of RKIP(S153E) is disordered in the structure. (C) Superposition of the RKIP solution structure (orange) and the X-ray crystal structure (gray). The C-terminal helix was excluded when the structures were superimposed. (D) Structural perturbations caused by the S153E mutation. Yellow spheres represent residues whose $^{1}H,^{15}N$ HSQC cross peak was significantly affected. Residues S153 (red) and P74 (blue) are also shown as spheres. (E) Structural perturbations caused by the P74L mutation, shown in the same manner as in panel D. (F) Residues whose amide proton is affected by DHPE binding (yellow spheres). (G) Residues exhibiting significant R_{ex} values (yellow spheres) (see Fig. S4C in the supplemental material). Residues P74 and S153 are indicated as reference points.

takes on the *cis* conformation, which is commonly observed for the amide bond preceding a Pro. Although the P74L mutation probably introduced a *trans* peptide bond at this location, because non-Pro residues strongly favor a *trans* bond, the HSQC spectrum of the P74L mutant showed only localized changes (see Fig. S2 in the supplemental material), and urea-induced denaturation experiments showed that the mutant is well folded under the conditions used for biochemical and NMR experiments (data not shown). The P74L mutation did not affect the S153 NMR peak, and the S153E mutation did not affect residues near P74, showing that there is no direct structural cross talk between the conserved P74 pocket site and the Raf-regulatory S153 phosphorylation site. We could not probe the P74 residue directly, because proline does not have an amide group and therefore cannot be detected by HSQC spectroscopy. Taken together, these results indicate that neither crystallography nor NMR reveals direct structural coupling between the P74 site in the pocket and the S153 phosphorylation site.

Although there is no apparent structural cross talk between P74 and S153, further analysis reveals a common region comprising the rim of the pocket that is influenced by mutations at both sites. A comparison of the HSQC spectra of wt RKIP and the phosphomimetic S153E mutant (see Fig. S2 in the supplemental material) identified structural perturbations to residues 142, 146, 147, and 150, which line the rim of the pocket and are located in a loop ("loop 127-150" [Fig. 3A]) immediately preceding the α-helix containing S153 (Fig. 3D). This loop is highly conserved among mammalian PEBPs (Fig. 4). While the P74L mutation did not affect the S153-containing α-helix, it also perturbed residues in the rim of the pocket, including residues in and adjacent to loop 127-150, as well as in the C-terminal α-helix (Fig. 3E and 4; see also Fig. S2 in the supplemental material). Both the crystallographic and the NMR data strongly suggest that wt RKIP is predominantly monomeric, and hence these structural perturbations occur within the RKIP monomer. Thus, it is possible that perturbations in the area around the P74L mutation, including the loop region lining the rim of the pocket, contribute to changes in the kinase binding and phosphorylation of RKIP.

NMR-based screening identified phospholipids as ligands for the RKIP pocket. The results described above demonstrated that mutations that alter pocket structure and/or dynamics can indirectly influence RKIP phosphorylation. To determine whether pocket occupancy also affects RKIP phosphorylation or target inhibition, we needed to identify a ligand that binds to the pocket. Therefore, we performed NMR-based screening in which protein HSQC peaks were used as site-specific probes for compound binding (36). A water-soluble, short-chain analogue of phosphatidylethano-

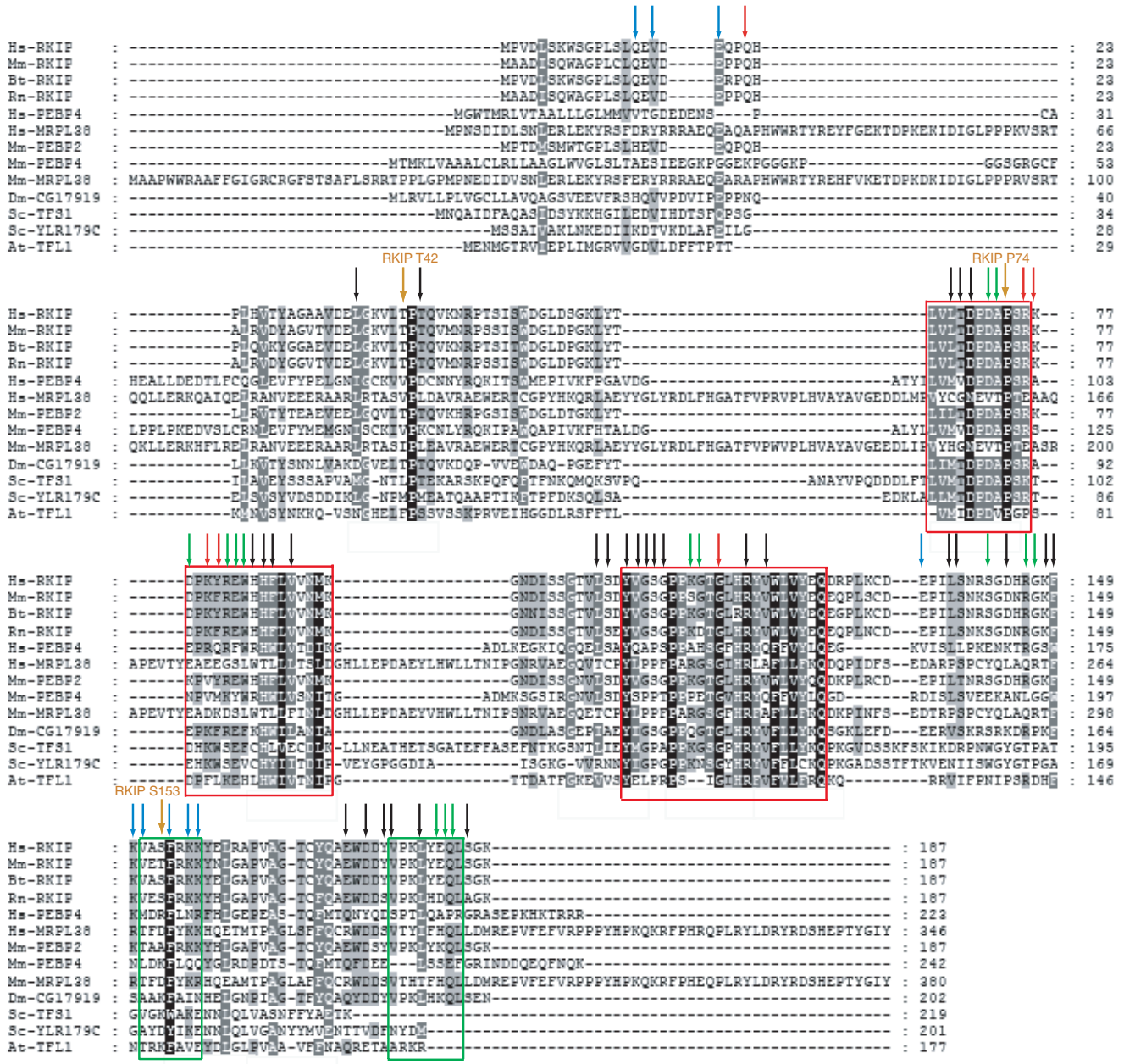

FIG. 4. Alignment of PEBP domain protein sequences from animals, plants, and budding yeast. Highly conserved regions (pocket) are outlined in red, and the S153 and C-terminal α-helices are outlined in green. The phosphorylation sites (T42 and S153) and the P74 site are marked. The arrows summarize the results of NMR experiments. Arrows indicate residues affected by either the S153E mutation (blue), the P74L mutation (red), lipid binding (black), or at least two of these three perturbations (green). The numbers refer to the amino acid numbers for rat RKIP/PEBP. Sequences are designated by species abbreviations followed by the homolog designation, GenBank GI number, or Ensembl gene name. Included are all rat, human, macaque, bovine, and mouse sequences, mammalian-sequence-related fly and worm sequences, SP-related *Arabidopsis thaliana* and tomato sequences, the yeast TFS1p sequence, two eubacterial sequences, and one archaeal sequence. Hs, *Homo sapiens*; Bt, *Bos taurus*; Dm, *Drosophila melanogaster*; Mm, *Mus musculus*; Rn, *Rattus norvegicus*; At, *Arabidopsis thaliana*; Sc, *S. cerevisiae*.

lamine, DHPE, binds RKIP (Fig. 3F and 5A to C), consistent with the ability of PEBP to bind phospholipids (39). DHPE is the first pocket-binding ligand characterized in solution at physiological pH. DHPE affected HSQC peaks for residues surrounding the pocket, indicative of binding to the pocket (Fig. 3F and 4). Longer fatty acid chains ($\geq C_8$) formed micelles, preventing similar NMR analysis. PE (the head group) binding was detected at acidic pHs but not at a neutral pH, suggesting that the head group without the aliphatic moieties is insufficient for measurable binding with a K_d lower than ~50 mM (Fig. 5G; low-pH data not shown). Consistent with a requirement for hydrophobic interactions at a neutral pH, DHPE and other short-chain phospholipids (phosphatidylserine, phosphatidylglycerol, and phosphatidic acid) bound comparably to the RKIP pocket (Fig. 5C to F). Finally, the P74L mutation does not significantly change the

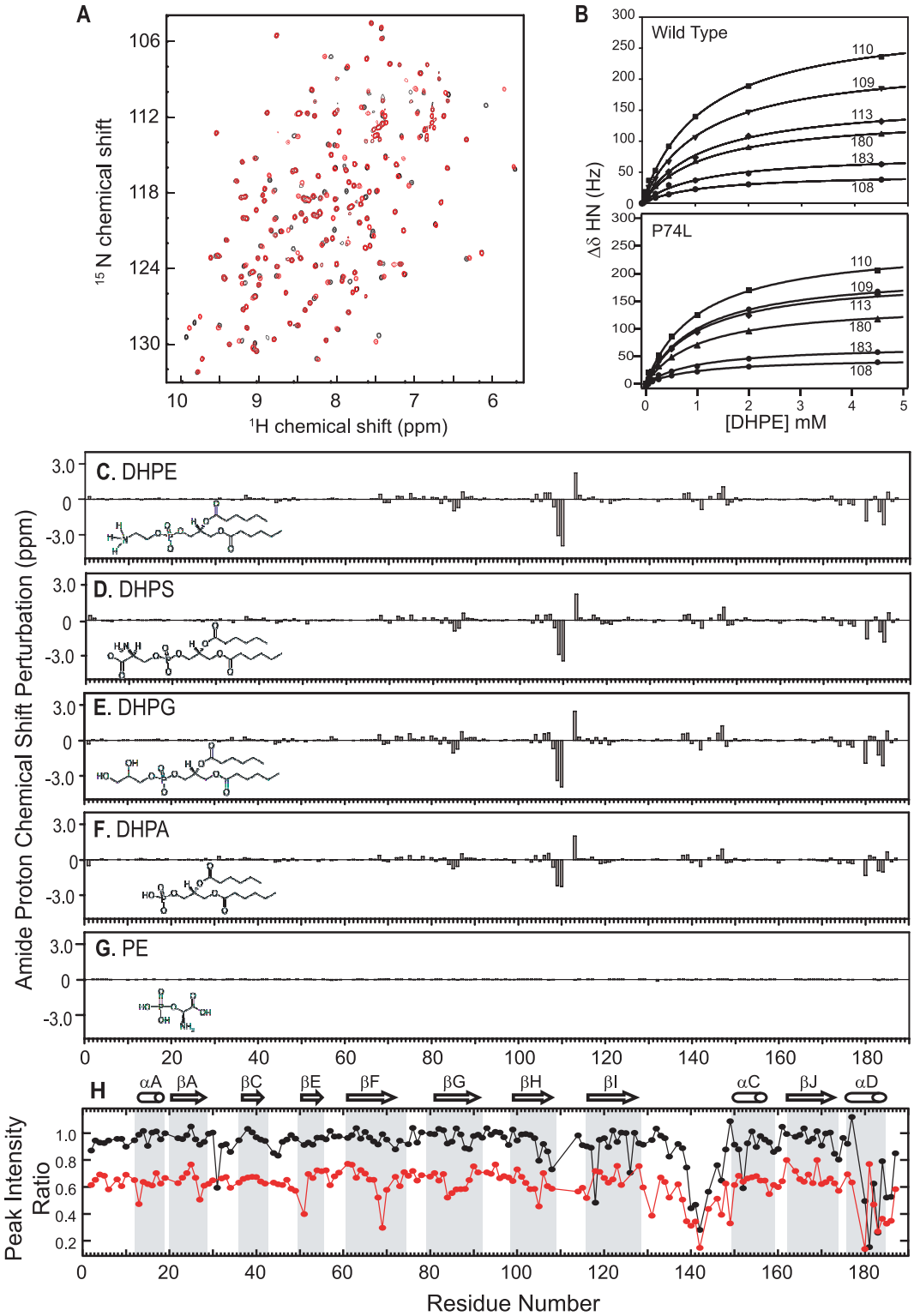

FIG. 5. Ligand binding of RKIP monitored by NMR spectroscopy. (A) Overlay of $^{1}H,^{15}N$ HSQC spectra of RKIP in the absence (black) and presence (red) of DHPE (4.5 mM). DHPE binding results in a number of chemical shift perturbations, indicating that the compound binds to RKIP in a site-specific manner. (B) Titration of DHPE binding to wt RKIP and RKIP(P74L). Changes in the amide ^{1}H chemical shift for the indicated residues are plotted versus DHPE concentrations. (C to G) RKIP chemical shift perturbations for amide proton resonances by DHPE (4.5 mM) (C), dihexanoylphosphatidylserine (DHPS; 4.5 mM) (D), dihexanoylphosphatidylglycerol (DHPG; 4.5 mM) (E), dihexanoylphosphatidic acid (DHPA; 4.5 mM) (F), and PE (10 mM) (G). The perturbations are plotted as a function of the residue number. The chemical structures of these compounds are also shown. (H) The ratios of the HSQC peak intensity of the apoprotein to that of the DHPE-bound protein are plotted versus residue numbers. Black circles, wt RKIP data; red circles, P74L mutant data. A low peak intensity ratio indicates that the HSQC peak of interest is weaker in the apoprotein than in the DHPE-bound protein. The secondary-structure elements are shown and labeled according to the designations used by Banfield et al. (3).

interaction with DHPE (K_d, 1.15 ± 0.05 mM for the wt and 1.03 ± 0.05 mM for the P74L mutant [Fig. 5B]), indicating that the mutation does not alter the structural elements of the pocket that are important for lipid binding. Since DHPE binds wt and mutant RKIPs comparably, we used it to analyze the effect of pocket occupancy on RKIP function.

Ligand binding to the pocket influences RKIP phosphorylation. To test the effect of ligand binding on RKIP phosphorylation, we initially monitored PKC phosphorylation of RKIP at S153. Although DHPE had no effect on the phosphorylation of a common PKC substrate, myelin basic protein (MBP) (Fig. 6A; see also Fig. S1A in the supplemental material), DHPE reduced the phosphorylation of RKIP by PKC. DHPE also decreased the phosphorylation of RKIP(P74L) by PKC with a comparable apparent 50% inhibitory concentration (IC_{50}) (85 ± 6 μM DHPE for the wt and 99 ± 10 μM DHPE for the P74L mutant) but to a lesser extent (Fig. 6A), indicating that the difference in the degree of inhibition was not due to differences in pocket occupancy. Analysis of the effect of DHPE is complicated by the observation that PKC activity is dependent on phospholipids, and DHPE activates PKC as a substitute for phosphatidylserine, a PKC activator (4) (see Fig. S1A in the supplemental material). Therefore, we also tested the effect of DHPE on RKIP phosphorylation by a lipid-independent kinase, ERK2 (Fig. 6B). As with PKC, the levels of phosphorylation of wt RKIP and RKIP(P74L) by ERK2 decreased to different extents upon DHPE binding but with similar IC_{50}s (223 ± 12 μM DHPE for the wt and 278 ± 10 μM DHPE for the P74L mutant) (Fig. 6B). Thus, in contrast to the P74L mutation, lipid binding to the RKIP pocket reduces its phosphorylation by kinases.

To investigate the mechanism in more detail, we examined the effect of DHPE on activated ERK2 binding to wt RKIP or RKIP(P74L) by using SPR. In agreement with its effects on catalytic activity, DHPE inhibited the binding of ERK2 to wt RKIP to a greater extent than its binding to RKIP(P74L) (Fig. 6C). The IC_{50} of DHPE against the binding of wt RKIP to ERK2 (321 ± 60 μM) was similar to its IC_{50} against the phosphorylation of wt RKIP. However, the IC_{50} against the binding of RKIP(P74L) to ERK2 was difficult to determine, due to the limited extent of inhibition; still, it should be comparable to that for wt RKIP, since both bind DHPE with similar affinities (see above). Incomplete inhibition of the RKIP-ERK2 interaction, as well as differential effects with mutant versus wt RKIP, suggests that DHPE is not a simple competitive inhibitor of RKIP phosphorylation.

To test this possibility directly, we analyzed the inhibition of ERK2 phosphorylation of wt RKIP by using various concentrations of DHPE at several fixed RKIP concentrations. Lineweaver-Burk plots generated for each DHPE concentration show a significant decrease in V_{max} values with increasing concentrations of the inhibitor as determined from the points of intersection with the *y* axis (Fig. 6D). On the other hand, no appreciable changes in the K_m were detected at different lipid concentrations. This pattern represents a noncompetitive model for DHPE inhibition of RKIP phosphorylation by ERK2. Pocket occupancy influences the binding of RKIP to kinases, contributing to an eventual decrease in RKIP phosphorylation.

Ligand binding to the pocket inhibits RKIP–Raf-1 interaction. Does phospholipid binding to the pocket also affect RKIP interaction with its target, Raf-1? To address this question, we determined whether DHPE competes with RKIP for binding to TAP-tagged Raf-1. DHPE prevented Raf-1 association with both wt RKIP and RKIP(P74L). The IC_{50}s of 614 ± 45 μM and 640 ± 48 μM, respectively, were similar to the K_ds for DHPE binding determined by NMR (Fig. 7A). In contrast to the effects of DHPE on RKIP phosphorylation described above, no differential effect in Raf-1 binding was found between wt RKIP and RKIP(P74L), suggesting that localized structural changes near the mutation were not critical for Raf-1 interaction. DHPE similarly decreased the binding of GST-RKIP to a bacterially expressed, CBP-tagged Raf kinase domain (see Fig. S1C in the supplemental material). These results reveal that a hydrophobic phospholigand, such as a soluble membrane phospholipid mimic, competes with Raf-1 for pocket binding and thus represents an alternative mechanism for regulating RKIP function. Furthermore, the inhibition by the pocket ligand suggests that the binding of Raf-1 to RKIP is influenced by pocket occupancy.

The pocket is flexible. The functional analyses described above have established that the RKIP pocket can interact with at least three distinct classes of targets: small-molecule ligands (e.g., DHPE), Raf-1, and other kinases that phosphorylate RKIP (e.g., PKC and ERK2). The existing crystal structures of apo-RKIP and RKIP-anion complexes are highly similar, and they do not provide a clear mechanism for the ability of RKIP to interact with a variety of partners. As a first step toward addressing this question, we characterized the solution structure of RKIP using NMR spectroscopy.

In the course of the ligand binding characterization described above, we found the first evidence for the flexible nature of the pocket. The shape of NMR peaks is a sensitive probe for millisecond time scale motions, and accordingly, the HSQC peak shape can be used to infer the relative mobility of specific RKIP residues. In the wt apoprotein, a number of residues exhibited significantly broadened HSQC peaks and consequently lower peak heights than the rest of the protein. DHPE binding sharpened these resonances and restored their intensities. These intensity changes are manifested in a peak intensity ratio (defined as the ratio of the intensity for the apoprotein to the intensity for the complex) of <1, as plotted in Fig. 5H. These are the residues located at the rim of the pocket, including most of residues 140 to 150 within loop 127-150 and those near the C-terminal end of the C-terminal α-helix. The ligand-induced peak sharpening suggests that these residues have higher mobility on the millisecond time scale in the apoprotein state than in the holoprotein state.

The same type of analysis of relative peak intensity for the P74L mutant revealed transient self-association of this mutant in addition to flexibility in the pocket. In addition to lower mean intensities for the same set of residues found for the wt as described above, there was a uniform decrease (~30%) in peak intensity across all residues for the P74L mutant apoprotein relative to that for the wt apo-RKIP (Fig. 5H). As described below, this uniform decrease in peak intensity is highly likely to be caused by weak, transient self-association of the P74L mutant. While lower peak intensity could be due to a decrease in conformational stability, a separate chemical denaturation experiment showed that the P74L mutant was well folded (data not shown), excluding this possibility. Together,

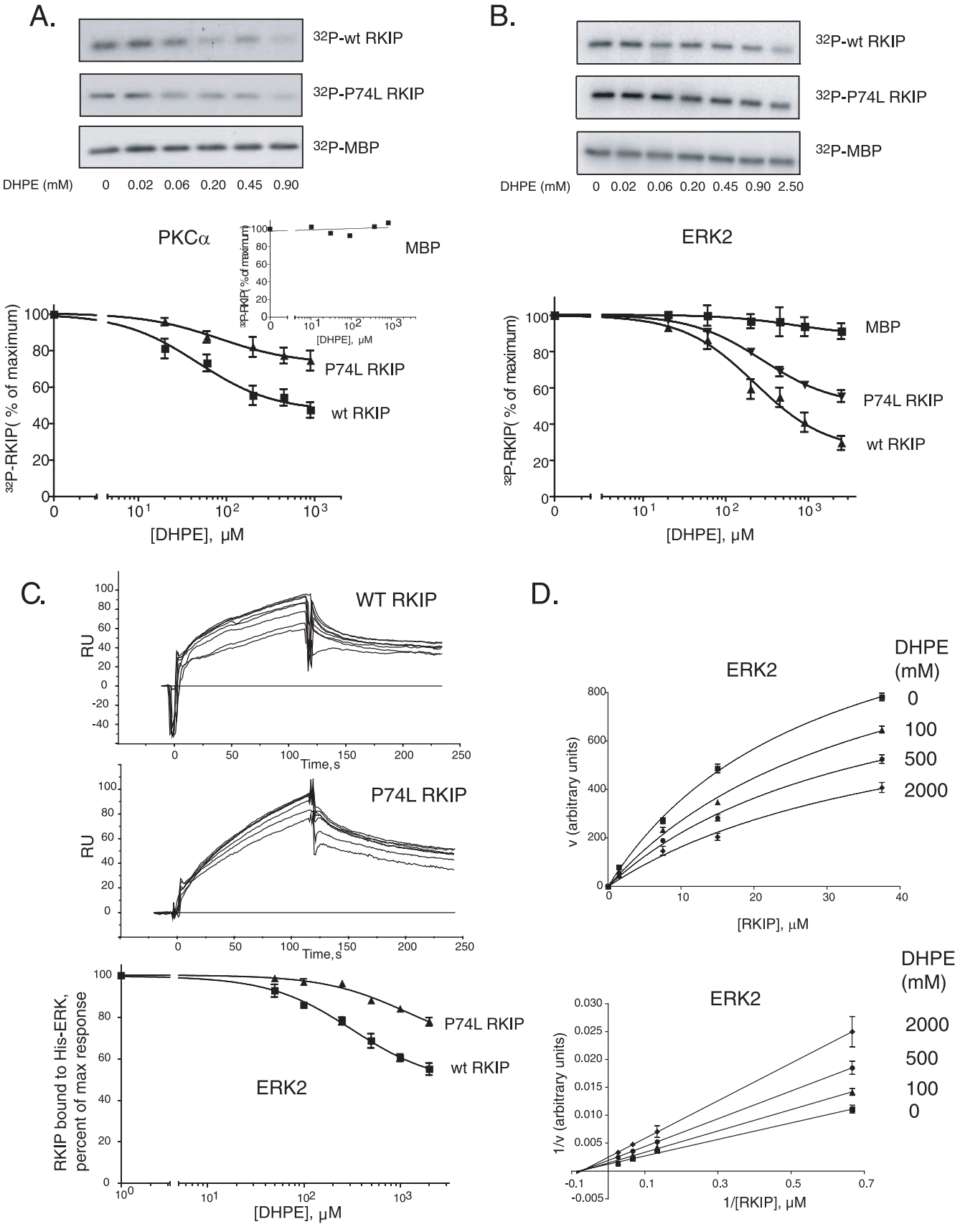
A.
32P-wt RKIP
32P-P74L RKIP
32P-MBP
DHPE (mM) 0 0.02 0.06 0.20 0.45 0.90
PKCα
MBP
32P-RKIP(% of maximum)
[DHPE], μM
P74L RKIP
wt RKIP
B.
32P-wt RKIP
32P-P74L RKIP
32P-MBP
DHPE (mM) 0 0.02 0.06 0.20 0.45 0.90 2.50
ERK2
MBP
P74L RKIP
wt RKIP
C.
WT RKIP
RU
Time,s
P74L RKIP
RKIP bound to His-ERK, percent of max response
ERK2
D.
ERK2
DHPE (mM)
0
100
500
2000
v (arbitrary units)
[RKIP], μM
1/v (arbitrary units)
1/[RKIP], μM

these results strongly suggest that in both wt RKIP and RKIP(P74L), the residues constituting the rim of the pocket and those near the C-terminal α-helix exhibit a significant level of mobility, and that DHPE binding decreases this mobility.

More in-depth characterization of conformational dynamics using ^{15}N relaxation experiments (Fig. 7B to D; see also Fig. S3 in the supplemental material) confirmed that the regions in apo-RKIP identified above as flexible (i.e., the C-terminal α-helix and loop 127-150) are indeed significantly mobile in the microsecond and millisecond time scales (Fig. 3G). These residues exhibited a significant rate constant for chemical exchange (R_{ex}) in the "model-free" analysis of ^{15}N relaxation data, which is indicative of motions in the microsecond-millisecond time scales (27). These residues also exhibited small but significant degrees of relaxation dispersion behavior in the constant-time Carr-Purcell-Meiboom Gill experiments (see Fig. S4 in the supplemental material). The small dispersion indicates that the rate of the chemical exchange reaction is greater relative to the effective field strength used in the experiments (2 kHz), making more in-depth analysis impossible. In contrast, the order parameter values (S^2) for the residues in loop 127-150, which are sensitive to motions in the picosecond-nanosecond time scales, were similar to those for the rest of the protein (Fig. 7B), indicating that the loop is not disordered. However, the N terminus of the protein exhibited significantly reduced S^2 values. Because of the low affinity and limited solubility of the lipids, it was not possible to prepare an RKIP sample where the pocket is fully saturated with ligand. Consequently, it was not possible to directly compare the ^{15}N relaxation properties of the apo- and holo-RKIPs. Nevertheless, these results, taken together, strongly suggest that the pocket in the apoprotein form is well structured but adopts multiple conformations through motions in the microsecond-millisecond time scales.

^{15}N relaxation measurements of RKIP(P74L) gave additional signs of its very weak self-association. Its ^{15}N R_2 (transverse relaxation) values exhibited a uniform increase over the respective wt RKIP values, characteristic of a larger effective size (data not shown), and analytical ultracentrifugation revealed a small amount of a higher-molecular-weight species in the P74L mutant but not the wt RKIP sample at protein concentrations used for NMR studies (≥0.2 mM [data not shown]). These properties prevented detailed analysis of the conformation dynamics of the P74L mutant. Although the self-association at extremely high protein concentrations is probably not biologically relevant, it indicates that the P74L mutation alters surface properties, consistent with the enhanced affinity of RKIP(P74L) for PKC and ERK2 shown above. However, we cannot rule out the possibility that the oligomerization triggered by the P74L mutation forms a new binding surface that enhances enzyme interactions.

Finally, the NMR-derived solution structure of apo-RKIP revealed structural features that are consistent with pocket flexibility. While the global fold of apo-RKIP in the crystal structure is retained in solution, the C-terminal helix points more outward in solution than in the crystal structure (Fig. 3C; see also Fig. S5 in the supplemental material). Although the NMR chemical shifts indicate that the C-terminal helix forms in solution (see Fig. S5A to C in the supplemental material), residues in this helix exhibited no significant protection of their amide protons in amide H-D exchange measurements (Fig. 7E). This lack of protection indicates marginal conformational stability of the hydrogen-bonded structure of the C-terminal helix, as expected for a highly solvent exposed helix, supporting the small but significant structural difference found in the NMR-derived structure. The residues in loop 127-150 also exhibited no significant protection in amide H-D exchange, as expected from a flexible region that is not involved in α-helix or β-sheet formation.

DISCUSSION

The ability of the RKIP binding pocket to integrate two signals, kinase phosphorylation and ligand binding, provides two distinct roles for the pocket in controlling RKIP function. First, the pocket mutation or ligand binding affects RKIP association with and phosphorylation by kinases. Second, ligand binding to the pocket inhibits RKIP–Raf-1 interaction. RKIP structural analyses revealed that the residues in the rim of the pocket adopt multiple conformations in the microsecond-millisecond time scale; thus, the pocket is capable of changing its shape. This finding is significant for two reasons. First, it provides a structural basis for the broad binding spectrum of the pocket. We have shown that the pocket is capable of binding to chemically distinct ligands, including the lipid DHPE and the polypeptide Raf-1. The conformational plasticity of the pocket is likely to be required for forming distinct sets of interactions for such chemically diverse ligands. Second, the ability to alter conformation is the basis of allostery. Our observation that DHPE noncompetitively inhibits the ERK2-catalyzed phosphorylation of RKIP suggests allosteric coupling between ligand binding to the pocket and RKIP-kinase interactions. The presence of the significant conformational dynamics in the

FIG. 6. DHPE binding decreases wt RKIP and RKIP(P74L) interactions with PKC and ERK2 in vitro. (A and B) Phosphorylation of wt RKIP and the P74L mutant by PKC (A) and ERK2 (B) was carried out in the presence of increasing concentrations of DHPE using RKIP, RKIP(P74L), or MBP as the substrate. (Top) Representative Western blots; (bottom) graphs of results from four independent experiments ± standard deviations. (A, inset) Graph of MBP phosphorylation. (C) The kinetics of wt RKIP (5 μM) and RKIP(P74L) (1 μM) interactions with ERK2 in the presence of increasing concentrations of DHPE (50 to 2,000 μM) were analyzed by SPR in a Biacore 3000 apparatus. (Top and center) The association and dissociation phases for wt RKIP and RKIP(P74L) were monitored for 120 s. (Bottom) The arbitrary response units (RU) at the 115-s point during the association phase were plotted using a one-site competition equation. The graph shows results from three independent experiments ± standard deviations. (D) Kinetics of wt RKIP phosphorylation by ERK2 in the presence of various concentrations of DHPE. (Bottom) Double-reciprocal plot of the data. The K_m and V_{max} values calculated from the fitting curves were 28.7 ± 2.8 μM and 1,384 ± 72 arbitrary units (AU) without DHPE, 37.2 ± 4.8 μM and 1,280 ± 96 AU with 100 μM DHPE, 36.5 ± 5.7 μM and 1,029 ± 93 AU with 500 μM DHPE, and 39.6 ± 12.0 μM and 873 ± 141 AU with 2,000 μM DHPE, respectively.

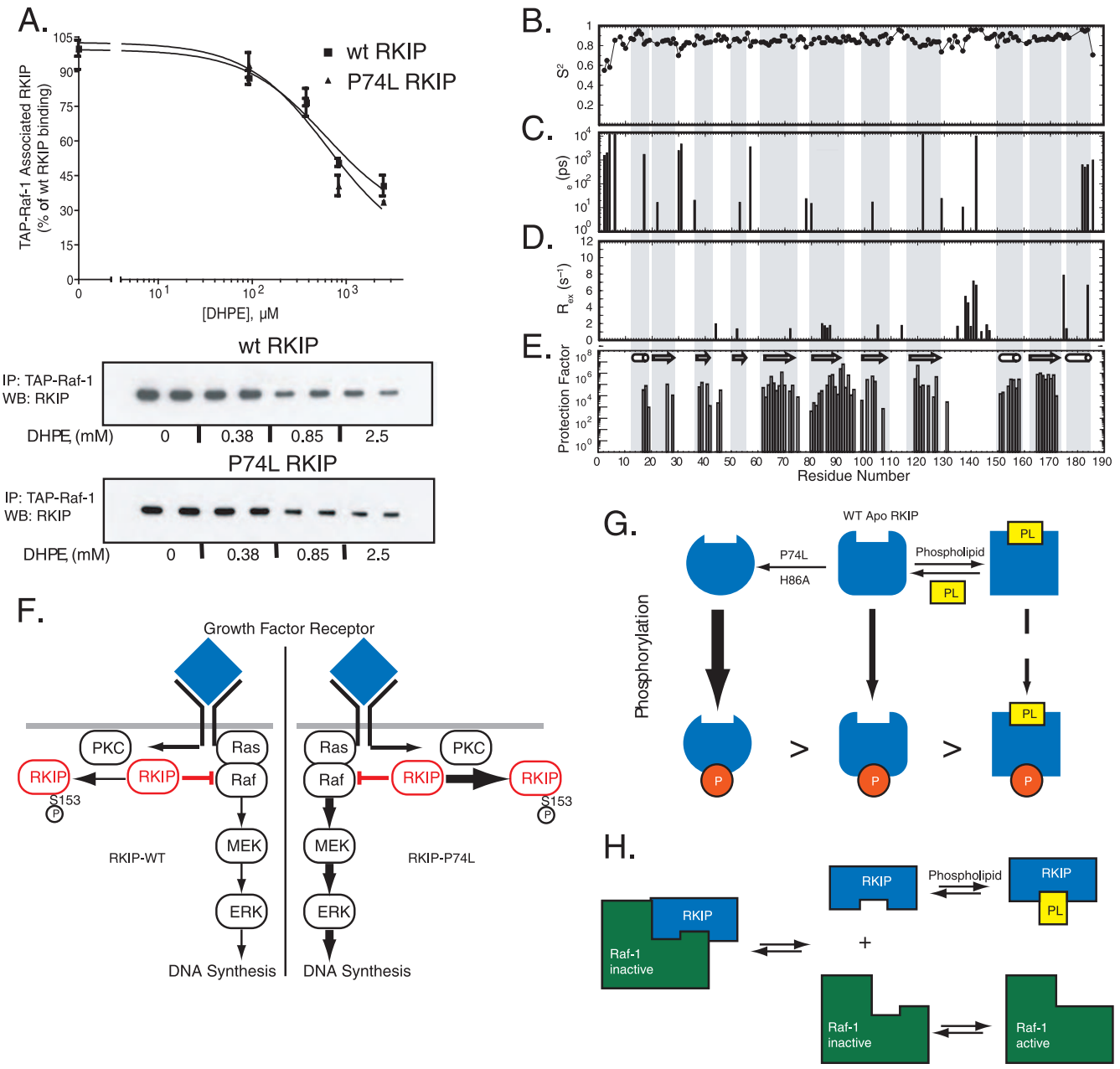

FIG. 7. (A) Effect of DHPE on Raf-1–RKIP interaction. TAP-Raf-1 was immunoprecipitated (IP) from stable H19-7 TAP-Raf-1 cells using IgG Sepharose and was incubated with soluble wt RKIP or RKIP(P74L) in the presence of different concentrations of DHPE. (Top) Graph of results from three independent experiments ± standard deviations. Data for RKIP binding to Raf-1 are expressed as percentages of wt RKIP binding to Raf-1 in the absence of DHPE. (Bottom) Representative Western blot (WB) of RKIP. (B to E) Backbone dynamics and stability of wt apo-RKIP. Model-free parameters were derived from an analysis of the ^{15}N relaxation data according to an axially symmetric model. The order parameter (S^2) (B), the correlation time for the rapid internal motions (t_e) (C), R_{ex} (D), and amide H-D exchange protection factors (E) are plotted versus residue numbers. A large protection factor indicates a stable local structure. (F) Schematic showing regulation of growth factor receptor signaling by RKIP and the effect of the RKIP pocket mutation on the pathway. In unstimulated cells, RKIP binds to Raf-1 and functions as an inhibitor. Upon cell stimulation by growth factors and activation of receptors such as the EGF receptor, RKIP is phosphorylated by PKC at S153. Phosphorylated RKIP then dissociates from Raf-1, which allows Raf-1 activation of MEK and MAPK (ERK). The P74L mutation leads to increased RKIP phosphorylation, thus facilitating signaling downstream of Raf-1. (G) Schematic showing that phospholipid (PL) binding to the ligand-binding pocket competitively prevents RKIP association with Raf-1. Following RKIP dissociation, Raf-1 is activated by phosphorylation. (H) Schematic showing that the pocket regulates RKIP inhibition of Raf-1 by modulating RKIP phosphorylation. The P74L mutation confers greater flexibility on the pocket and tail regions of the protein and enables more-efficient phosphorylation of RKIP. Phospholipid association with RKIP leads to a more rigid structure around the pocket and decreases RKIP phosphorylation. Phosphorylation of RKIP at S153 prevents RKIP binding to and inhibition of Raf-1.

pocket rim provides a physical mechanism for such allosteric coupling.

A model for the regulation of RKIP is shown in Fig. 7. In mammalian cells, PKC phosphorylation of RKIP at S153 prevents its association with Raf-1, enabling Raf-1 to be phosphorylated by activating kinases (38). This regulatory mechanism is critical for MAPK activation, since the RKIP(S153V) mutant stabilizes the RKIP–Raf-1 interaction and inhibits MAPK sig-

naling in cells (8). The P74L pocket mutation potentiates phosphorylation at S153, reducing the amount of RKIP bound to Raf-1 and thereby inactivating its inhibitory function (Fig. 7F). Pocket ligands such as DHPE and other phospholipids can also affect RKIP interaction with kinases. DHPE noncompetitively inhibits the kinase binding and phosphorylation of RKIP (Fig. 7G). This mechanism, observed for PKC, MAPK, and other RKIP kinases, enables RKIP ligands to modulate RKIP phosphorylation by multiple kinases. In addition, pocket ligands block RKIP interaction with Raf-1 (Fig. 7H). Unlike its inhibition of kinases, lipid binding prevents RKIP association with its target, Raf-1, independently of pocket mutation. Interestingly, RKIP is not an inhibitor for the kinases that phosphorylate it. One possible explanation consistent with our results is that inhibitory targets of RKIP bind directly to the pocket, whereas kinases that phosphorylate RKIP do not bind directly to the pocket but are sensitive to its conformation and/or flexibility. These data raise the possibility that other modifications of RKIP, such as phosphorylation at other residues, may also indirectly affect S153 phosphorylation and RKIP binding to Raf-1 via subtle changes in pocket structure and/or dynamics. Thus, the pocket may act as a sensor as well as a regulator of RKIP phosphorylation and function.

The noncompetive inhibition of RKIP phosphorylation by DHPE suggests a mechanism reminiscent of the allosteric regulation of enzymes. Interestingly, the P74L mutation affects kinase binding but not lipid binding to RKIP. This result is consistent with the noncompetitive nature of the DHPE inhibition, whereby the site of lipid binding is distinct from the site of kinase binding. Ligand binding to wt RKIP and ligand binding to the P74L pocket mutant have opposite effects on RKIP interaction with kinases and subsequent RKIP phosphorylation. This observation could be explained if residues involved in kinase binding and/or phosphorylation are perturbed in opposite ways by pocket mutation versus DHPE binding. There is a significant overlap between the RKIP residues perturbed by ligand binding and those perturbed by the P74L mutation, and it is likely that some of these residues are involved in the kinase interaction.

The mechanism of RKIP regulation by the pocket that we have elucidated is a novel one that has not been described previously. RKIP is distinct from the p21/p27 class of kinase inhibitors and from well-characterized interaction domains. p21 and p27 are natively unfolded proteins and bind to cyclin-dependent kinase–cyclin complexes in an extended form (25, 26). Although they are also controlled by phosphorylation (17), they do not possess a pocket that regulates their phosphorylation. The size of RKIP is similar to that of many interaction domains involved in signal transduction (31). Although interaction domains such as SH2 are globular and possess a target-binding pocket, they function primarily as rigid-body modules (12, 24). RKIP most closely resembles receiver domains involved in bacterial signal transduction (40). These single-domain allosteric proteins exhibit large changes in conformational dynamics upon phosphorylation by an upstream kinase. However, RKIP appears to be unique in that it possesses a pocket that controls its efficacy as a kinase substrate and as an interacting protein inhibitor.

The fact that DHPE binds to the pocket and prevents Raf-1 association implicates at least some of these pocket residues directly or indirectly in the interaction between RKIP and Raf-1. Since we have mapped all the perturbations in the pocket caused by DHPE binding at physiological pH, it should be possible to identify more precisely the RKIP residues involved in Raf-1 binding. Previous studies from our laboratory have shown that RKIP binding to Raf-1 blocks the phosphorylation of sites in the S338-to-Y341 region of Raf-1, and that conversely, mutation of these S338-to-Y341 phosphorylation sites prevents RKIP binding to Raf-1, implicating this region on Raf-1 as the site of RKIP interaction (38). More-recent mutational and peptide studies of Raf-1 are consistent with these results (30). Following submission of this article, a recent report also found that pocket mutation of RKIP affects MAPK signaling (32a). However, in contrast to the conclusion of those investigators, we demonstrate that differential binding of Raf-1 to the pocket is not responsible for the loss of mutant RKIP function in cells. A possible reason for this discrepancy is that those authors used a small, phosphorylated peptide to probe Raf-1 binding to RKIP and described only subtle changes in binding. However, further studies are required to define the exact nature of RKIP interaction sites with targets such as Raf-1 and kinases such as PKC or ERK2.

Previous studies have suggested that RKIP associates with synthetic phospholipid bilayers via peripheral, electrostatic interactions and that the association involves both the C-terminal and N-terminal regions of RKIP rather than the pocket (39). We have also tested RKIP association with synthetic phospholipid bilayers and did not observe significant RKIP insertion (data not shown). We used DHPE because it is the longest alkyl chain lipid we could find that was water soluble and did not form micelles. We do see tighter association of RKIP with longer alkyl chain lipids, but they also form micelles (data not shown), which may lead to nonspecific interactions. Finally, it is possible that specific lipids within the bilayer may bind to RKIP with higher affinity. Therefore, the overall physiological significance of lipid binding is unclear, and further investigation is needed to resolve this point.

The work presented here not only provides a new paradigm for the regulation of signaling cascades but also enhances the potential of RKIP as a therapeutic target by characterizing important mutants and enabling targeted drug development. The ability of RKIP to regulate MAPK signaling and its role in controlling the metastatic potential of multiple cancer cell types make it an exciting target for therapeutic intervention. The pocket-dependent regulation of RKIP function by phospholipid-like molecules can be exploited in developing small chemicals that could ultimately lead to intervention for diseases related to dysregulation of pathways involving RKIP and/or RKIP targets.

ACKNOWLEDGMENTS

We thank W.-J. Tang, P. Nash, B. Roux, S.-H. Shiu, and A. Lin for helpful discussions, J. Kurutz and J. Wojcik for assistance in NMR data collection, and L. Zeng for help with gene annotation. We are particularly grateful to M. Cobb for generously supplying ERK2 protein.

This work was supported by grants from the National Institutes of Health (NS33858 and CA112310; to M.R.R.), the Howard Hughes Medical Institute Research Resources Grant (to M.R.R. and S.K.), the University of Chicago Cancer Research Center (to M.R.R. and S.K.), and a gift from the Cornelius Crane Trust for Eczema Research (to M.R.R.).

REFERENCES

1. **Akaishi, J., M. Onda, S. Asaka, J. Okamoto, S. Miyamoto, M. Nagahama, K. Ito, O. Kawanami, and K. Shimizu.** 2006. Growth-suppressive function of phosphatidylethanolamine-binding protein in anaplastic thyroid cancer. Anticancer Res. **26:**4437–4442.
2. **Al-Mulla, F., S. Hagan, A. I. Behbehani, M. S. Bitar, S. S. George, J. J. Going, J. J. Garcia, L. Scott, N. Fyfe, G. I. Murray, and W. Kolch.** 2006. Raf kinase inhibitor protein expression in a survival analysis of colorectal cancer patients. J. Clin. Oncol. **24:**5672–5679.
3. **Banfield, M. J., J. J. Barker, A. C. Perry, and R. L. Brady.** 1998. Function from structure? The crystal structure of human phosphatidylethanolamine-binding protein suggests a role in membrane signal transduction. Structure **6:**1245–1254.
4. **Bazzi, M. D., and G. L. Nelsestuen.** 1990. Protein kinase C interaction with calcium: a phospholipid-dependent process. Biochemistry **29:**7624–7630.
5. **Chatterjee, D., Y. Bai, Z. Wang, S. Beach, S. Mott, R. Roy, C. Braastad, Y. Sun, A. Mukhopadhyay, B. B. Aggarwal, J. Darnowski, P. Pantazis, J. Wyche, Z. Fu, Y. Kitagwa, E. T. Keller, J. M. Sedivy, and K. C. Yeung.** 2004. RKIP sensitizes prostate and breast cancer cells to drug-induced apoptosis. J. Biol. Chem. **279:**17515–17523.
6. **Chautard, H., M. Jacquet, F. Schoentgen, N. Bureaud, and H. Benedetti.** 2004. Tfs1p, a member of the PEBP family, inhibits the Ira2p but not the Ira1p Ras GTPase-activating protein in *Saccharomyces cerevisiae*. Eukaryot. Cell **3:**459–470.
7. **Clark, M. C., D. McElheny, J. Wojcik, J. Kurutz, M. R. Rosner, and S. Koide.** 2006. NMR assignment of rat Raf kinase inhibitor protein. J. Biomol. NMR **36**(Suppl. 1)**:**4.
8. **Corbit, K. C., N. Trakul, E. M. Eves, B. Diaz, M. Marshall, and M. R. Rosner.** 2003. Activation of Raf-1 signaling by protein kinase C through a mechanism involving Raf kinase inhibitory protein. J. Biol. Chem. **278:** 13061–13068.
9. **Cornilescu, G., F. Delaglio, and A. Bax.** 1999. Protein backbone angle restraints from searching a database for chemical shift and sequence homology. J. Biomol. NMR **13:**289–302.
10. **Eves, E. M., P. Shapiro, K. Naik, U. R. Klein, N. Trakul, and M. R. Rosner.** 2006. Raf kinase inhibitory protein regulates Aurora B kinase and the spindle checkpoint. Mol. Cell **23:**561–574.
11. **Eves, E. M., M. S. Tucker, J. D. Roback, M. Downen, M. R. Rosner, and B. H. Wainer.** 1992. Immortal rat hippocampal cell lines exhibit neuronal and glial lineages and neurotrophin gene expression. Proc. Natl. Acad. Sci. USA **89:**4373–4377.
12. **Farrow, N. A., R. Muhandiram, A. U. Singer, S. M. Pascal, C. M. Kay, G. Gish, S. E. Shoelson, T. Pawson, J. D. Forman-Kay, and L. E. Kay.** 1994. Backbone dynamics of a free and phosphopeptide-complexed Src homology 2 domain studied by ^{15}N NMR relaxation. Biochemistry **33:**5984–6003.
13. **Farrow, N. A., O. Zhang, J. D. Forman-Kay, and L. E. Kay.** 1995. Comparison of the backbone dynamics of a folded and an unfolded SH3 domain existing in equilibrium in aqueous buffer. Biochemistry **34:**868–878.
14. **Fu, Z., Y. Kitagawa, R. Shen, R. Shah, R. Mehra, D. Rhodes, P. J. Keller, A. Mizokami, R. Dunn, A. M. Chinnaiyan, Z. Yao, and E. T. Keller.** 2006. Metastasis suppressor gene Raf kinase inhibitor protein (RKIP) is a novel prognostic marker in prostate cancer. Prostate **66:**248–256.
15. **Fu, Z., P. C. Smith, L. Zhang, M. A. Rubin, R. L. Dunn, Z. Yao, and E. T. Keller.** 2003. Effects of Raf kinase inhibitor protein expression on suppression of prostate cancer metastasis. J. Natl. Cancer Inst. **95:**878–889.
16. **Granovsky, A. E., and M. R. Rosner.** 2008. Raf kinase inhibitory protein: a signal transduction modulator and metastasis suppressor. Cell Res. **18:**452–457.
17. **Grimmler, M., Y. Wang, T. Mund, Z. Cilensek, E. M. Keidel, M. B. Waddell, H. Jakel, M. Kullmann, R. W. Kriwacki, and L. Hengst.** 2007. Cdk-inhibitory activity and stability of $p27^{Kip1}$ are directly regulated by oncogenic tyrosine kinases. Cell **128:**269–280.
18. **Grzesiek, S., and A. Bax.** 1993. The importance of not saturating H_2O in protein NMR. Application to sensitivity enhancement and NOE measurements. J. Am. Chem. Soc. **115:**12593–12594.
19. **Hagan, S., F. Al-Mulla, E. Mallon, K. Oien, R. Ferrier, B. Gusterson, J. J. Garcia, and W. Kolch.** 2005. Reduction of Raf-1 kinase inhibitor protein expression correlates with breast cancer metastasis. Clin. Cancer Res. **11:** 7392–7397.
20. **Huang, X., X. Yang, B. J. Luft, and S. Koide.** 1998. NMR identification of epitopes of Lyme disease antigen OspA to monoclonal antibodies. J. Mol. Biol. **281:**61–67.
21. **Kay, L. E., P. Keifer, and T. Saarinen.** 1992. Pure absorption gradient enhanced heteronuclear single quantum correlation spectroscopy with improved sensitivity. J. Am. Chem. Soc. **114:**10663–10665.
22. **King, A. J., H. Sun, B. Diaz, D. Barnard, W. Miao, S. Bagrodia, and M. S. Marshall.** 1998. The protein kinase Pak3 positively regulates Raf-1 activity through phosphorylation of serine 338. Nature **396:**180–183.
23. **Knuesel, M., Y. Wan, Z. Xiao, E. Holinger, N. Lowe, W. Wang, and X. Liu.** 2003. Identification of novel protein-protein interactions using a versatile mammalian tandem affinity purification expression system. Mol. Cell. Proteomics **2:**1225–1233.
24. **Kristensen, S. M., G. Siegal, A. Sankar, and P. C. Driscoll.** 2000. Backbone dynamics of the C-terminal SH2 domain of the p85α subunit of phosphoinositide 3-kinase: effect of phosphotyrosine-peptide binding and characterization of slow conformational exchange processes. J. Mol. Biol. **299:**771–788.
25. **Kriwacki, R. W., L. Hengst, L. Tennant, S. I. Reed, and P. E. Wright.** 1996. Structural studies of p21Waf1/Cip1/Sdi1 in the free and Cdk2-bound state: conformational disorder mediates binding diversity. Proc. Natl. Acad. Sci. USA **93:**11504–11509.
26. **Lacy, E. R., I. Filippov, W. S. Lewis, S. Otieno, L. Xiao, S. Weiss, L. Hengst, and R. W. Kriwacki.** 2004. p27 binds cyclin-CDK complexes through a sequential mechanism involving binding-induced protein folding. Nat. Struct. Mol. Biol. **11:**358–364.
27. **Lipari, G., and A. Szabo.** 1982. Model-free approach to the interpretation of nuclear magnetic resonance relaxation in macromolecules. 1. Theory and range of validity. J. Am. Chem. Soc. **104:**4546–4559.
28. **Lorenz, K., M. J. Lohse, and U. Quitterer.** 2003. Protein kinase C switches the Raf kinase inhibitor from Raf-1 to GRK-2. Nature **426:**574–579.
29. **Nallamsetty, S., R. B. Kapust, J. Tozser, S. Cherry, J. E. Tropea, T. D. Copeland, and D. S. Waugh.** 2004. Efficient site-specific processing of fusion proteins by tobacco vein mottling virus protease in vivo and in vitro. Protein Expr. Purif. **38:**108–115.
30. **Park, S., O. Rath, S. Beach, X. Xiang, S. M. Kelly, Z. Luo, W. Kolch, and K. C. Yeung.** 2006. Regulation of RKIP binding to the N-region of the Raf-1 kinase. FEBS Lett. **580:**6405–6412.
31. **Pawson, T., and P. Nash.** 2003. Assembly of cell regulatory systems through protein interaction domains. Science **300:**445–452.
32. **Pnueli, L., L. Carmel-Goren, D. Hareven, T. Gutfinger, J. Alvarez, M. Ganal, D. Zamir, and E. Lifschitz.** 1998. The SELF-PRUNING gene of tomato regulates vegetative to reproductive switching of sympodial meristems and is the ortholog of CEN and TFL1. Development **125:**1979–1989.

32a. **Rath, O., S. Park, H. H. Tang, M. J. Banfield, R. L. Brady, Y. C. Lee, J. D. Dignam, J. M. Sedivy, W. Kolch, and K. C. Yeung.** 2008. The RKIP (Raf-1 kinase inhibitor protein) conserved pocket binds to the phosphorylated N-region of Raf-1 and inhibits the Raf-1-mediated activated phosphorylation of MEK. Cell Signal. **20:**935–941.

33. **Schoentgen, F., and P. Jolles.** 1995. From structure to function: possible biological roles of a new widespread protein family binding hydrophobic ligands and displaying a nucleotide binding site. FEBS Lett. **369:**22–26.
34. **Schuierer, M. M., F. Bataille, S. Hagan, W. Kolch, and A. K. Bosserhoff.** 2004. Reduction in Raf kinase inhibitor protein expression is associated with increased Ras-extracellular signal-regulated kinase signaling in melanoma cell lines. Cancer Res. **64:**5186–5192.
35. **Serre, L., B. Vallee, N. Bureaud, F. Schoentgen, and C. Zelwer.** 1998. Crystal structure of the phosphatidylethanolamine-binding protein from bovine brain: a novel structural class of phospholipid-binding proteins. Structure **6:**1255–1265.
36. **Shuker, S. B., P. J. Hajduk, R. P. Meadows, and S. W. Fesik.** 1996. Discovering high-affinity ligands for proteins: SAR by NMR. Science **274:**1531–1534.
37. **Stols, L., M. Gu, L. Dieckman, R. Raffen, F. R. Collart, and M. I. Donnelly.** 2002. A new vector for high-throughput, ligation-independent cloning encoding a tobacco etch virus protease cleavage site. Protein Expr. Purif. **25:**8–15.
38. **Trakul, N., R. E. Menard, G. R. Schade, Z. Qian, and M. R. Rosner.** 2005. Raf kinase inhibitory protein regulates Raf-1 but not B-Raf kinase activation. J. Biol. Chem. **280:**24931–24940.
39. **Vallee, B. S., P. Tauc, J. C. Brochon, R. Maget-Dana, D. Lelievre, M. H. Metz-Boutigue, N. Bureaud, and F. Schoentgen.** 2001. Behaviour of bovine phosphatidylethanolamine-binding protein with model membranes. Evidence of affinity for negatively charged membranes. Eur. J. Biochem. **268:** 5831–5841.
40. **Volkman, B. F., D. Lipson, D. E. Wemmer, and D. Kern.** 2001. Two-state allosteric behavior in a single-domain signaling protein. Science **291:**2429–2433.
41. **Wilsbacher, J. L., and M. H. Cobb.** 2001. Bacterial expression of activated mitogen-activated protein kinases. Methods Enzymol. **332:**387–400.
42. **Yeung, K., T. Seitz, S. Li, P. Janosch, B. McFerran, C. Kaiser, F. Fee, K. D. Katsanakis, D. W. Rose, H. Mischak, J. M. Sedivy, and W. Kolch.** 1999. Suppression of Raf-1 kinase activity and MAP kinase signalling by RKIP. Nature **401:**173–177.
43. **Yeung, K. C., D. W. Rose, A. S. Dhillon, D. Yaros, M. Gustafsson, D. Chatterjee, B. McFerran, J. Wyche, W. Kolch, and J. M. Sedivy.** 2001. Raf kinase inhibitor protein interacts with NF-κB-inducing kinase and TAK1 and inhibits NF-κB activation. Mol. Cell. Biol. **21:**7207–7217.
44. **Zheng, D., Y. J. Huang, H. N. Moseley, R. Xiao, J. Aramini, G. V. Swapna, and G. T. Montelione.** 2003. Automated protein fold determination using a minimal NMR constraint strategy. Protein Sci. **12:**1232–1246.